Biophys Struct Mech (1981) 8: 67–93

Biophysics of Structure and Mechanism

Light-Induced Axial and Radial Shrinkage Effects and Changes of the Refractive Index in Isolated Bovine Rod Outer Segments and Disc Vesicles

Physical Analysis of Near-Infrared Scattering Changes

K. P. Hofmann, A. Schleicher, D. Emeis, and J. Reichert

Institut für Biophysik und Strahlenbiologie der Universität Freiburg im Breisgau, Albertstrasse 23, D-7800 Freiburg i. Br., Federal Republic of Germany

Abstract. Flash-induced transients in the near-infrared scattering of bovine rod outer segments and isolated discs are investigated. Their common characteristic is the saturation at a rhodopsin bleaching of ca. 10%, which was previously described for the so-called "signal *P*". The theory is based on the Rayleigh-Gans-approximation and on a cylindrical particle shape. This treatment is shown to be applicable in the measured angular range (in general $\theta \leq 30°$), in spite of the polydisperse shape of the real particles. Using the angular dependence of the relative intensity change (difference scattering curve), changes of the polarizability (refractive index) and of the particle shape can be distinguished. Model difference scattering curves are calculated for the dimensions of the rod outer segments. Static scattering measurements are used for an estimation of the average particle shape: the isolated disc samples appear to contain flat discs as well as an admixture of rod-like structures (ca. 1% of the total scattering mass); in rod outer segment preparations, a contribution of non-rodlike scattering is found which is strongly dependent on the treatment of the sample. The flash induced transients were measured using randomly oriented particles (discs and rod outer segments) and axially oriented rod outer segments. The angular dependence of the amplitude yields its difference scattering curve. On suspensions of isolated discs, which were re-loaded with the proteins extracted at low ionic strength, one single signal is observed (termed P_D, first order, $\tau = 0.6-1.2$ s). Using randomly oriented rod outer segments, a signal with complex millisecond kinetics (termed signal *P*) and a slow signal (termed P_S, first order, $\tau = 5-25$ s) can be distinguished kinetically. In the axially oriented rod outer segments, the *P*-signal splits into a fast axial (10 ms) and a slower radial component (50–100 ms). The slow signal P_S observed in ROS and the signal P_D in discs have one common physical interpretation as local changes of the polarizability, directly observed in light-scattering as a change of the refractive index. The fast signal *P* in ROS,

Abbreviations: ROS: rod outer segments; RGA: Rayleigh-Gans-approximation

0340-1057/81/0008/0067/$ 05.40

however, has no detectable local component but represents a pure shrinkage effect. On the axially oriented system, this shrinkage turns out to be axial and radial with different kinetics. Only rough estimations for the relative shrinkage effects and refractive index changes can be given. One obtains for 1% rhodopsin bleaching:

$$\frac{\Delta n}{n} \approx 10^{-4}, \quad \frac{\Delta L}{L} \approx 10^{-2}, \quad \frac{\Delta R}{R} \approx 5 \times 10^{-4}.$$

Assuming a fluid plane for the disc membrane, the planar shrinkage induced by one bleached rhodopsin is estimated from the radial shrinkage as ca. 300 Å^2. This high value is discussed in relation to the binding of rhodopsin to the GTP-binding protein which is involved in comparable effects described by Kühn et al. (1981). According to our data, a chemical binding process in milliseconds is only indicated in the isolated disc; in the closed disc stack of the rod outer segment, only weak (fast) local interactions are consistent with the difference scattering data. A turn or lift of the GTPase would better satisfy this condition and explain the above high value for the individual shrinkage effect.

Key words: Kinetic light-scattering – Flash photometry – Rod outer segments – Disc membrane – Rhodopsin

Introduction

It is possible to detect rapid transients in the structure of cell organelles by kinetic light-scattering photometry. We demonstrated this for bovine rod outer segments (Hofmann et al. 1976). The structure changes, however, are most likely not essential for the function of the cell, but only serve as sensitive indicators for structure-, especially membrane-bound processes. There is a causal connection between the underlying molecular event (e.g., chemical binding), the indicator process (e.g., change of the refractive index) and the monitoring signal. The variety of possible indicator processes is as large as the physical changes influencing light-scattering. It is therefore necessary to specify the indicator processes for every measured signal.

For one of the light-scattering transients found in rod outer segments, the so-called *P*-signal (Hofmann et al. 1976), the indicator process was described as a "shrinkage" of the disc organelles densely packed within the outer segment (Uhl et al. 1977).

We are now able to distinguish three different "*P*-signals" in rod outer segments and one in discs: they have all the same characteristic dependence on light, i.e., they are only observed when no more than 15% of the rhodopsin is bleached in the sample by preceding illumination. In tens of minutes, the effects are recovered (Hofmann and Schnetkamp unpublished).

The *P*-signals must be distinguished from the negative *N*-signal which is proportional to bleaching (Hofmann et al. 1976). Signals with a saturation at less

than 1% bleaching are also observed (Hofmann et al. 1976; Schnetkamp and Hofmann unpublished).

This study will characterise and distinguish the *P*-signals by their specific indicator processes and by their kinetics. Furthermore, the ROS-signals are compared with a signal observed on isolated disc vesicles.

Materials and Methods

Measuring Device

To monitor the scattered light, the scattering part of the combined scattering- and absorption device was used which was described previously (Hofmann and Emeis 1981).

For isotropic samples (randomly oriented ROS and discs), we used two different selection optics for the scattering angle:

1. The Fresnel lenses and ring diaphragms as described in the previous investigation, setup schematically shown in Fig. 1a.
2. A half-spherical self-focussing cuvette and half-spherical detector array, developed from a similar device previously described (Hofmann et al. 1976) and schematically shown in Fig. 1c. This apparatus will be described in more detail elsewhere. It is connected to four channels of the signal analyser for the simultaneous measurement at four different scattering angles.

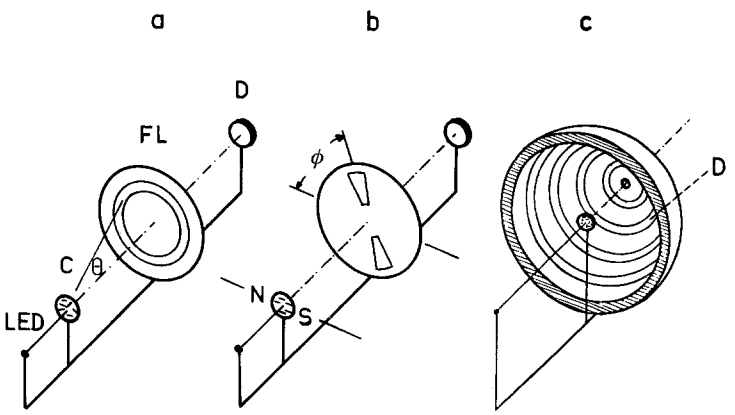

Fig. 1a–c. Geometry of light-scattering detection. **a** Isotropic sample. The parallel incident light, coming from the LED source, is scattered by the sample within the cuvette *C*; the scattered light is focussed onto the detector *D* by two large Fresnel lenses FL. Selection of one scattering angle θ by ring diaphragms, centrosymmetric to the optical axis. **b** Axially oriented rod outer segments. Selection of the scattering angle and an additional selection of the angle ϕ relative to the axis of the outer segments oriented in the magnetic field *N-S*; a wide range of θ is transmitted in the above schematic picture, sharper selections are also used in some experiments. **c** Isotropic sample, simultaneous measurement of several scattering angles. The cuvette is half-spherical, all parallel rays of scattered light, equal in θ, are focussed on the same detector array, centrosymmetric to the optical axis and located on the larger half-sphere. The signals from several scattering angles are simultaneously measured

Oriented ROS were measured with an arrangement shown in Fig. 1b. Oriented samples were produced by the field of a Bruker B-E10 research magnet. A quartz cuvette (diameter 20 mm, layer thickness 0.5 mm) is placed between the magnetic poles, the field strength at the sample is 12 kG. The horizontal scattering ($\phi = 0°$) and the vertical scattering ($\phi = 90°$) can be measured simultaneously using arrays of semiconductor detectors.

The false light caused by reflections of the primary beam was controlled by measuring the angular intensities for pure saline. Due to the high scattering intensities in the investigated angular range, the contribution of the false light could be kept below 20% at all angles. For the normalisation of the signals, the false intensities were subtracted from the measured static scattering intensities. The additional error of the signals due to the superimposed total scattering signal will be discussed in the theoretical section.

Preparation and Sample

The composition of the saline for preparation and measurement is: 130 mM KCl, 0.5 mM $MgCl_2$, 1 mM $CaCl_2$, 0.5 mM (Ethylene dinitrilo) – tetra acetic acid (EDTA), 1 mM Dithiothreitrol (DTT), 10 mM Piperazine – 1,4 – diethane sulfonic acid (PIPES). The preparation follows a standard procedure described in detail in a previous paper (Uhl et al. 1978); briefly, the retinae are shaken in isotonic saline solution, the suspension is filtered through a nylon mesh, layered on a discontinuous sucrose gradient and washed in saline.

Isolated discs were prepared according to Smith et al. (1975). 2,5% Ficoll was used instead of 5% to reduce side effects caused by Ficoll (Bauer and Mavromati 1980).

All measurements were performed within 3 h after preparation; within this time, the decrease of the scattering anisotropy (see below) is slow, and the light-induced effects are stable. The latter are also absolutely reproducible from one preparation to the other (see for example Fig. 11). Similar scattering effects were obtained with liquid *N*-frozen samples and with samples forced through glasswool. However, the scattering anisotropy was partially lost under these conditions, parallel to the radial and axial splitting of the light-induced effects (see section results, static scattering).

Common parameters of all measurements are: pH = 6.5; T = 22° C; rhodopsin concentration $5 \cdot 10^{-7}$ M; relative rhodopsin turnover per flash $\varrho = 0.02$, if not otherwise stated (Fig. 7).

Theory

1. General Considerations

The scattering of a suspension of bovine rod outer segments is very complex and cannot be treated rigorously. We shall first consider the so-called Rayleigh-Gans scattering and then discuss the strong limitations of this theory with respect to

our subject. The physical basis of the signals described in this study is that the interaction of the infrared monitoring light with the rod outer segment particles is changed by flash-induced processes. Since the particles don't absorb at $\lambda_m = 880$ nm, the refractive index is a real number. The monitoring light used has a coherence length of ca. 12 μm, long enough for the interference of scattered light from different parts of a particle.

Two quite different processes which influence the scattering can be distinguished: either the "scattering power" of the "scattering centers" or their distance and therefore the phase shift and interference of the scattered rays is changed. This study distinguishes between these two events by their angular dependence: the former is in the allowed approximation not angular dependent whereas a sharp dependence is expected for the latter. A further criterion will be given by the dependence on orientation. The following deductions are based on the classical treatment of light-scattering as found in the textbooks of van de Hulst (1957) and Kerker (1969).

2. Rayleigh-Gans Approximation

The Rayleigh-Gans approximation considers only the geometrical phase shift between the rays coming from different scattering centers; this means that the following assumptions are made: The refractive index of the particles is, measured relative to that of the medium, close to one:

$$|m - 1| \ll 1. \quad m = \frac{n_{\text{particle}}}{n_{\text{medium}}}; \tag{1}$$

the phase shift due to the length of the light path, which is different for different rays, has to be negligible:

$$2\,ka|m - 1| \ll 1\,, \tag{2}$$

a: dimension of the particle, $k = \dfrac{2\pi}{\lambda}$

In the RGA, the scattering intensity can be written as the product of a refractive index-dependent term and a θ-dependent term which contains the interference of the different elementary scattering waves.

For unpolarised incident light, one obtains:

$$I(\theta) = \frac{V^2 k^4}{r^2} \left(\frac{m - 1}{2\pi}\right)^2 \left(\frac{1 + \cos^2\theta}{2}\right) \cdot P(\theta,\phi)\,, \tag{3}$$

V = particle volume; r = distance from the particle, ϕ as in Fig. 1.
(3) is valid under the Rayleigh-Gans conditions (1), (2), and contains in addition the assumptions of isotropy and homogeneity of the scattering particle. We will discuss these restrictions separately in Sect. 5.

3. Difference Scattering

a) Total Scattering Signal. In kinetic scattering, as much quanta as possible must be detected in short times, in order to obtain a high signal to noise ratio. Due to the dependence of the signals on illumination, we cannot enhance it by averaging. This means that a compromise must be found between a high scattering intensity, i.e., concentration, and the distortion of the scattering curve with increasing concentration because of multiple scattering. Up to a total scattering of 20%, the scattering curves can still be interpreted. In the scattering differences, the total scattering effect will be superimposed to all the light-scattering in any direction: so to say, the individual incident light for any particle is not constant for all particles but is dependent on time and on its localization within the cuvette. The dependence of a signal on the scattering angle decides in which angular range the total scattering signal becomes predominant. Under our conditions, this is expected for small angles ($\theta \lesssim 5°$).

In one of the measurements of this study, the effect can be distinguished (Fig. 11).

b) Definition of the Transfer Function. Let x be a parameter influencing the scattering deduced in the last section. Then, for a small change Δx in this parameter and x_0 before the change:

$$\frac{\Delta I}{I}(\theta, x_0) = \frac{I(\theta, x_0 + \Delta x) - I(\theta, x_0)}{I(\theta, x_0)} = \left.\frac{\frac{\partial I(\theta, x)}{\partial x}}{I(\theta, x)}\right|_{x_0} \cdot \Delta x \tag{4}$$

is called (relative) difference scattering curve of the change in the parameter x. For convenience, a transfer function is defined

$$\gamma_x(\theta) = \frac{\Delta I}{I}(\theta) \cdot \left(\frac{\Delta x}{x}\right)^{-1} = \frac{x}{I} \cdot \frac{\partial I(\theta, x)}{\partial x}. \tag{5}$$

c) Transfer Function for a Change of the Refractive Index. It is assumed that Eq. (3) is valid. Then it follows with (5)

$$\gamma_m = \frac{2\,m}{m - 1}, \tag{6}$$

γ_m is independent of θ.

So far, the isotropic case was discussed. ROS, however, have an axial anisotropy, which, at least in frog ROS within the isolated preparation, is changed by light (Liebman et al. 1974). This effect could eventually be seen in light-scattering under our conditions. The signal must depend on the relative orientation of the rod axis to the polarization vector of linearily polarized light. This fact was used as an additional test.

d) Transfer Function for Shifts of the Scattering Mass. We assume now, that the individual scattering dipoles within the particle change only their mean distance. No scattering mass shall be lost. This is the case where only the function $P(\theta, \phi)$ in (3) is changed. The particle polarizability $(m-1)\ V$ remains thereby constant.

The general transfer function is:

$$\gamma_x(\theta) = \frac{x}{P(\theta, x)} \cdot \frac{\partial P(\theta, x)}{\partial x}. \tag{7}$$

Since $P(\theta) \to 1$ for $\theta \to 0$ (see for example Kratochvil 1972) independent of the distribution of scattering dipoles, the transfer function for a mass shift disappears for $\theta \to 0$.

$$\gamma_x(\theta) \to 0 \text{ for } \theta \to 0\,. \tag{8}$$

A comparison of (6) and (8) yields a good criterion for a distinction between mass shifts and changes of the refractive index.

4. Scattering of Discs

For discs, the Rayleigh-Gans approximation can be applied in the whole angular range $\theta \leqq 60°$. The scattering curve can be calculated after Kratky and Porod (see van de Hulst 1957). We used the more general formula (A5) given in the appendix as a rough measure for preparative deviations. The formula for the ellipsoidal shell given by Norisuye et al. (1977) was also used. It turned out that the special shape does not influence the scatterring for all flat forms, i.e., thickness or smaller semi-axis $\lesssim 500$ Å.

The scattering of our preparation will be considered in more detail in the section "static scattering". It suggests that mainly flat discs and an admixture of short cylinders, remaining from the original ROS, are present. Therefore, in Fig. 2, the difference scattering curves of a flat disc will be shown.

5. Scattering of ROS

A rigorous quantitative evaluation of the scattering and difference scattering of ROS is not possible. Some influences which can be expected to complicate the interpretation, shall now be discussed. Since ROS in vivo are best approximated by a circular cylinder, this geometry is chosen as the basic form.

a) Local and Non-Local Scattering Effects. The lamellar structure of the ROS is seen by light-scattering as a periodic change of the polarizability; it will be approximated by a sinusoidal axial modulation of the refractive index m:

$$m(z) - 1 = (\bar{m} - 1)\left(1 + b \cos \frac{2\pi z}{d}\right). \tag{9}$$

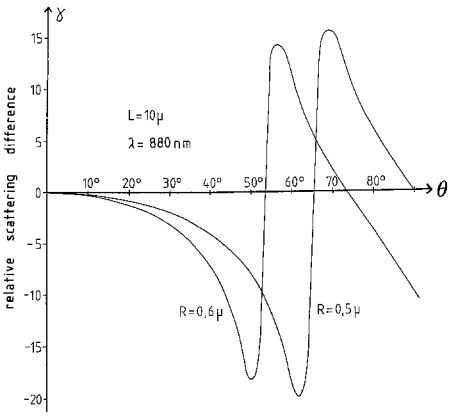

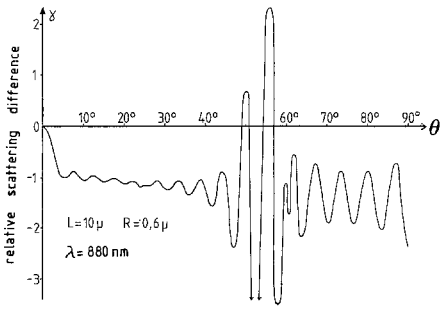

ΔR ROS, unoriented ΔL

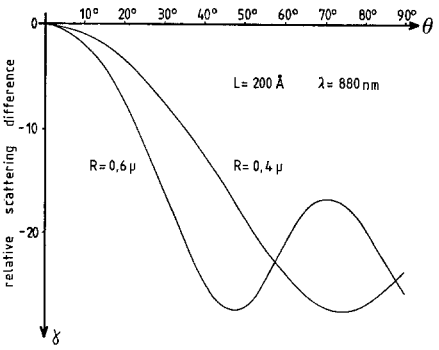

Discs

ΔR ROS, oriented ΔL

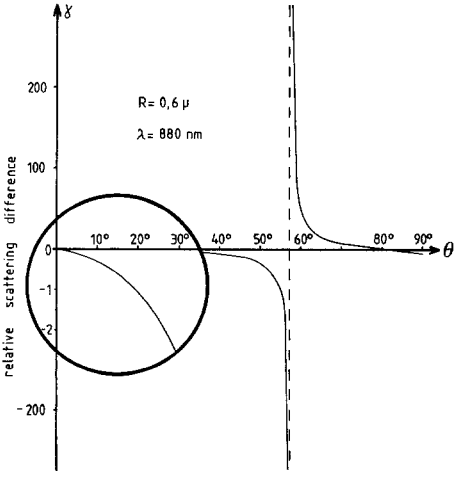

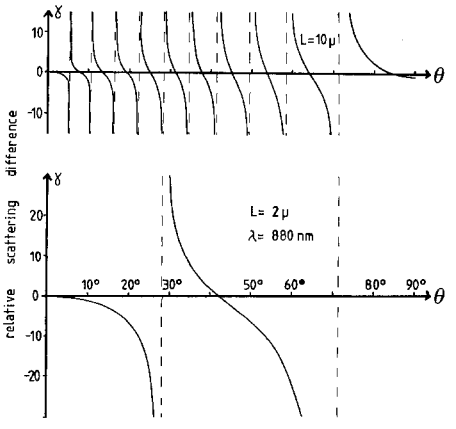

The period d was chosen $d = 300$ Å, the contrast factor $b = 0.8$. The scattering function is considered in the Appendix (A10–A11).

For the above values of b and d, the largest relative difference between the scattering of the lamellar and the homogeneous structure in the range $\theta < 30°$ was found to be 10^{-3}. Thus, the influence of lamellarity can be neglected and the solution for the homogeneous particle (3) can be used.

It results further, that two classes of effects can be distinguished:
1. Local effects, taking place within distances < 500 Å and uniformally distributed within the particle;
2. Non-local shifts of the scattering mass.

Real examples for the first kind would be chemical binding, as shown by Kühn et al. (1981), or changes in the package density of lipids, as shown for thermal phase transitions in lipid systems (Eibl and Blume 1979; Chong and Colbow 1976).

Real examples for shifts of the scattering mass are changes of the disc to disc repeat distance, shifts of peripheral proteins on the ROS membrane surface, or a crumpling or planar shrinkage of the disc membranes resulting in a decrease of the mean scattering radius of the ROS.

In general, local and non-local effects will be expected to be commonly reflected in one and the same real scattering signal. Local chemical binding, for example, could induce non-local effects via a change in the equilibrium of forces between the membranes in the disc stack. It is striking that the measured ROS-signals can be attributed rather specifically to local or non-local indicator processes.

b) Validity of the Rayleigh-Gans-Approximation. Using data by Liebman et al. (1974), a mean value for the relative refractive index of $m = 1.05$ is obtained for frog ROS. In spite of this low value, the general rule (2) shows that for ROS the Rayleigh-Gans-approximation (RGA) will not be valid in general. The error, however, increases with the scattering angle, and for sufficiently small angles, the RGA becomes valid for the geometry of the ROS. For very long cylinders under perpendicular incidence, Farone et al. (1963) calculated the exact solution and compared it with the RGA.

Due to the dominant radial scattering (see Fig. 5), the errors calculated for the long cylinders can also be used for the radial scattering of oriented ROS. It turns out that, for $m < 1.1$, the error of the RGA remains below 10% in the range $\theta \leq 20°$. For $20° \leq \theta \leq 30°$, extrapolation still yields errors smaller than 20%. Fortunately, these ranges coincide with those where a satisfying

---

Fig. 2. Calculated difference scattering curves for randomly oriented circular cylinders (above), circular discs (middle) and axially oriented circular cylinders (below). Dimensions are assumed as in bovine rod outer segments. Left side: small radial shrinkage; right side: small axial shrinkage. The transfer function γ defined in (11) is plotted, calculation following the Rayleigh-Gans-approximation. The random orientation of the particles in the upper curves smears out the sharp details, which are seen in the curves below, the poles are replaced by maxima. In the curve in the lower right corner, a length of 2 μm is tentatively assumed to simulate small coherent disc packets ("tiger stripes")

measurement of oriented ROS can be performed and where enough measuring points are available to distinguish between changes of refractive index (6) and shape effects (8). The radial scattering, therefore, can be quantitatively interpreted with the RGA.

The axial scattering is expected to be more difficult, because of the large axial dimension of the particles. Also in this case, the phase shifts for oriented ROS are relatively small in the angular range $\theta \leq 30°$. A comparison with the experimental curve (Fig. 5) suggests that the real axial scattering of the ROS follows essentially the RGA in this range.

Concerning the scattering differences, there are indications that the validity of the RGA extends further than for the static scattering-itself. For example see Fig. 7, where the characteristic constant difference scattering, which is expected in the RGA for a change of the refractive index, is observed even for randomly oriented ROS in the whole measured range $\theta \leq 60°$. For special approximations I (m) of the exact solution, this result can be understood, since the error of the transfer function (5) then is minimal in a large range. For the interpretation of the data, the range $\theta \leq 30°$ is sufficient; therefore, the problem was not further investigated.

The real axial difference scattering of ROS seems to be a special case, in so far as the curve appears to represent mainly mass shifts in dimensions much shorter than the ROS length. This point will be discussed further in the results (Fig. 11).

c) Influence of Polydispersity. Consider for the following Fig. 5 and the angular range around 15°. For a long straight cylinder, the axial scattering is nearly extinguished by interference and only radial scattering is observed. The ratio of anisotropy is still higher than 20 for cylinders as short as 5 μm (radius 0.5 μm). This is not only found for the Rayleigh-Gans scattering, but also for the general solution (van de Hulst 1957). For shorter cylinders, the axial scattering will increase and, therefore, the ratio of anisotropy decrease. The ratio is also expected to decrease when the cylinders become curved (but still oriented along an average axis), because of the presence of larger radial dimensions and the resulting steeper slope of the radial scattering.

Phase contrast microscopy shows that a fraction of the ROS is really curved and polydisperse with short lengths. However, the anisotropy ratio, which can be used as a sensitive average measure for that fraction, is as high as 8 for good preparations (c.f. Fig. 5 and Table 1). Thereby, it is verified that the straight cylinder is a reasonable choice for the basic form.

d) Calculations. For the calculations, overall shape changes, i.e., changes of radius or length of ideal cylinders are assumed. In view of the rather poorly defined preparation, only a few values of the transfer functions will be used as real pieces of information for the interpretation of the data. It is, however, interesting to compare the different transfer functions for changes of the diameter of discs and randomly or axially oriented ROS or to consider the influence of different diameters or lengths. For this purpose, some of the computed difference curves are shown in Fig. 2.

Table 1. Scattering anisotropy, i.e., the ratio between the scattered intensities vertical and horizontal to the rod axis, scattering angle $\theta = 10° \pm 2°$. The influence of storage time [(1)–(3)] and some other treatments are shown [(4)–(6)]. The values of the anisotropy are the average of four preparations

Sample	Anisotropy
(1) Immediately after preparation	8.0
(2) 3 h after preparation (stored at 0°)	6.7
(3) 6 h after preparation (stored at 0°)	6.0
(4) As (1), then osmotically shocked and resuspended in an isotonic milieu	2.5
(5) As (1), then treated with glasswool	5.0
(6) As (1), then frozen in liquid nitrogen and thawed	4.7

The scattering functions of oriented cylinders were calculated using the general formulae (A3) and (A4) given in the appendix; for the randomly oriented cylinder, one has to integrate over all orientations; the calculated curves are shown in Figs. 4 and 5, together with experimental data.

To calculate the difference scattering, formulae (A6)–(A9) are used.

Results

Orientation of the ROS in a Magnetic Field

ROS are axially oriented in a magnetic field [Chalazonitis, cited by Chabre (1975) who already used oriented ROS]. From the calculations in the theoretical section, it is expected that the light-scattering of ROS will be orientation sensitive. In the optical setup shown in Fig. 1b, an intensity change, caused by a change in the average orientation, can be measured. In the following experiment, the field and the detection were horizontal ($\phi = 0°$). Figure 3 shows the drastic effect after turning on the magnetic field during one second. It is interesting to note that the orientation effect is different for the bleached and the unbleached sample; this is possibly related to the illumination-dependent effect seen with frog ROS in a rotating magnetic field (Chabre 1978).

In order to make quite sure that the effect in Fig. 3 really reflects orientation an additional test with polarized light in the range $350 \leq \lambda \leq 700$ nm was made. Due to the dichroism of the disc stacks, the superposition of a scattering and an absorption effect is then observed. This total photometric effect is similar to that shown in Fig. 3; up to a constant, its amplitude, plotted as a function of the measuring wavelength, matches the absorption spectrum of rhodopsin. This shows that the unbleached disc stacks (rhodopsin is in a fixed orientation with respect to the rod axis) really become oriented.

Static Scattering

Discs. In Fig. 4, calculated and measured curves for discs are compared to each other. Most of the particles appear to scatter as flat disc; the range where the

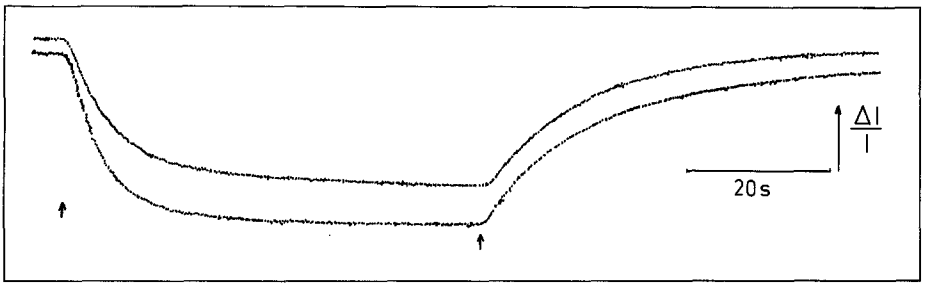

Fig. 3. Orientation of bovine rod outer segments in a magnetic field. Upper trace: unbleached, lower trace: thoroughly bleached. The field is turned on (during ca. 1 s) at the first and turned off at the second arrow. The orientation effect is strongly dependent on the preparation and related to the scattering anisotropy; see Fig. 6 and Table 1. Ratios of the intensities at the arrows between 2.5 and 8 are found. It is seen that the orientation is completed in about 1 min

particles can be considered as flat is discussed in the theoretical section. The elevation of the experimental curve at small angles is reasonably approximated by a 1% mass fraction of 1–2 μm particles. It appears that not all ROS are completely dissolved into single discs.

ROS. The factors which complicate the interpretation of the scattering of real ROS are discussed in the theoretical section. Only the relatively well defined scattering of oriented particles will be considered.

In Fig. 5, calculated and measured scattering curves are compared to each other. The sharp maxima of the calculated axial scattering cannot be observed with real ROS, due to the considerable polydispersity of the ROS length. The moderate coherence of our monitoring light may also smear out such details. The overall slope of the axial scattering, however, indicates that an axial dimension of 5–10 μm is correctly translated.

The high theoretical splitting of the axial and radial intensities is not observed experimentally. The decrease of the scattering anisotropy will be the higher the more the real ROS particles deviate from the ideal long and straight form. As is seen in Table 1, this can be used to derive a convenient criterion for the average geometrical quality of a preparation. Fresh and carefully prepared samples are indicated by a high scattering anisotropy.

Flash-Induced Scattering Signals

All signals are evoked by the first flash, applied on a fresh aliquot. The *N*-signal was subtracted following the procedure described in a previous paper (Hofmann and Emeis 1981). Apart from this, no further corrections were made.

1. Randomly Oriented Samples

a) ROS. Flash-induced signals of randomly oriented ROS were measured with the device shown in Fig. 1a and, independently, with the half-spherical

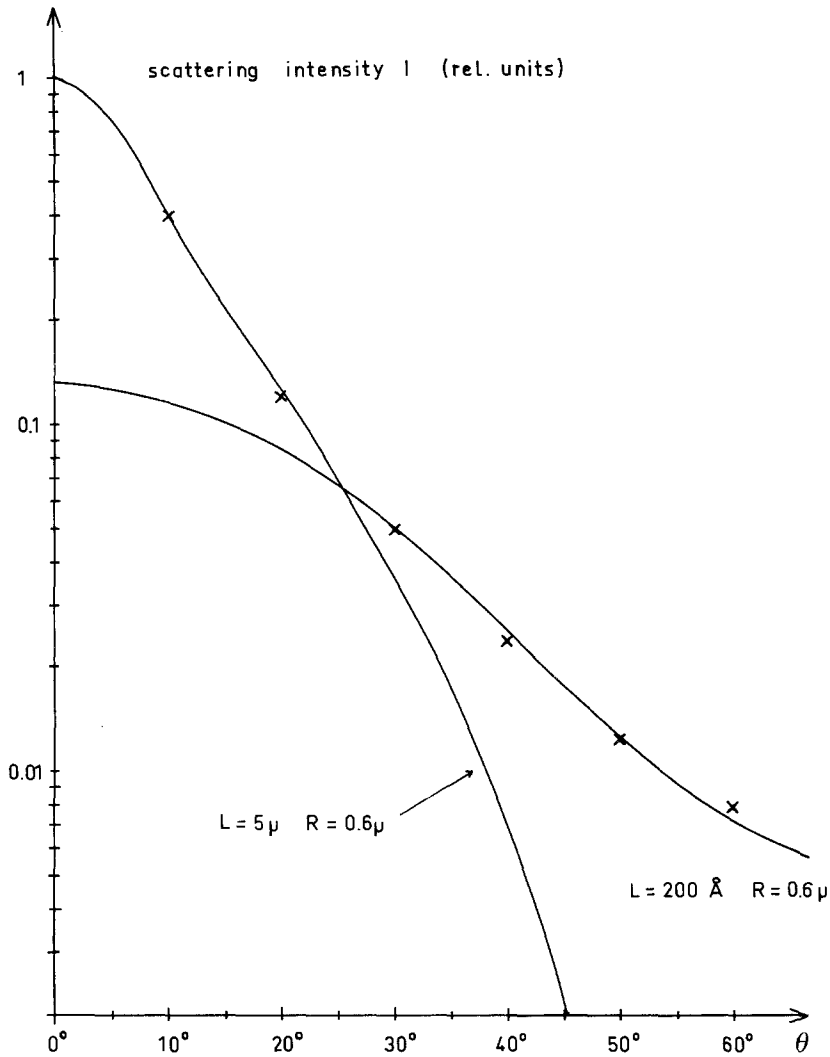

Fig. 4. Comparison of calculated and measured absolute scattering curves for isolated disc vesicles. It is seen that the measured values cannot be approximated by the lower curve for thin discs; the superposition of the scattering of short cylinders (upper curve) is able to explain the high measured values at small angles

arrangement shown in Fig. 1c. *P*-signals are shown in Fig. 6, being measured as transmission changes using randomly oriented ROS. Two light-induced effects can be distinguished in this way, one of them in the ms-range, called signal *P*, and a slower one, called signal P_S.

In the measurable angular range, the signals are kinetically comparable to those shown in Fig. 6. The slow signal P_S and the fast signal *P* are separated as in Fig. 6 and their amplitudes are plotted versus the scattering angle.

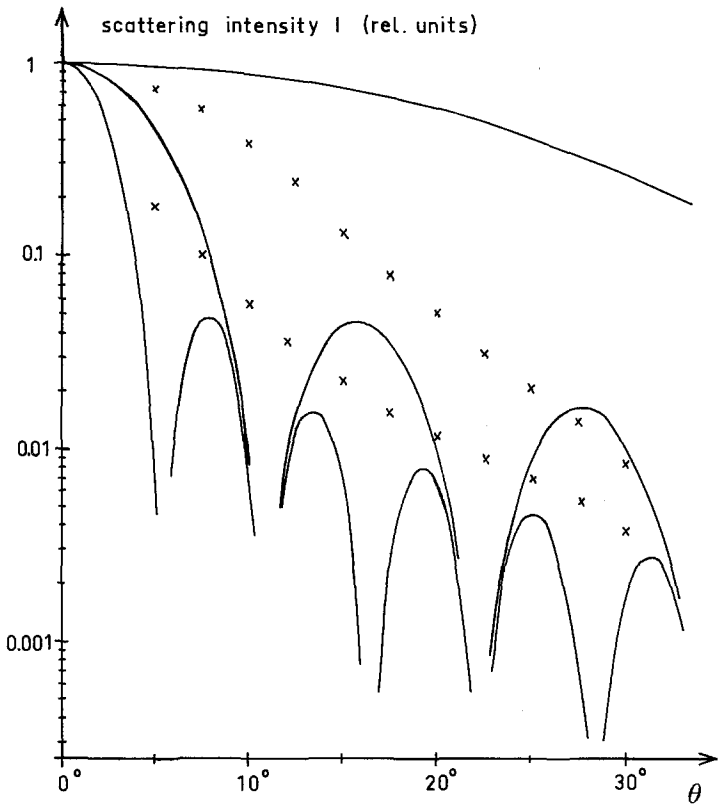

Fig. 5. Comparison of calculated and measured absolute scattering curves for axially oriented particles. Calculation of circular cylinders (R = 0.5 μm), measurement of a bovine rod outer segment suspension in a magnetic field of 12 kG (arrangement as in Fig. 1b). Upper solid curve: radial scattering; lower solid curve: axial scattering (broad maxima: L = 5 μm; sharper maxima: L = 10 μm). Upper crosses are scattered vertical intensities ($\phi = 90°$ in Fig. 1b), lower crosses are horizontal intensities ($\phi = 0°$ in Fig. 1b). It is seen that the measured scattering anisotropy is ca. 8 at $\theta = 10°$, which is by a factor of about five lower than the theoretical anisotropy of ideal cylinders

The resulting difference scattering curve for the amplitude of the separated slow signal P_S is shown in Fig. 7. The values are best approximated by a constant which is in accordance with the theoretical curve of a change in refractive index (6). Strikingly, the difference curve is constant also for higher angles where, in the absolute scattering, the Rayleigh-Gans-approximation is no longer valid. This point was considered in more detail in the theoretical section.

Concerning now the ms-signal, the difference scattering curve is quite different: as far as a reliable measurement of the scattering difference is possible, a steep increase with the scattering angle is found.

b) Discs. With discs, prepared as described above, no *P*-signal is observed. When, however, following a suggestion by Kühn (1981), the proteins extracted at low ionic strength are added, a large effect is obtained which is shown in

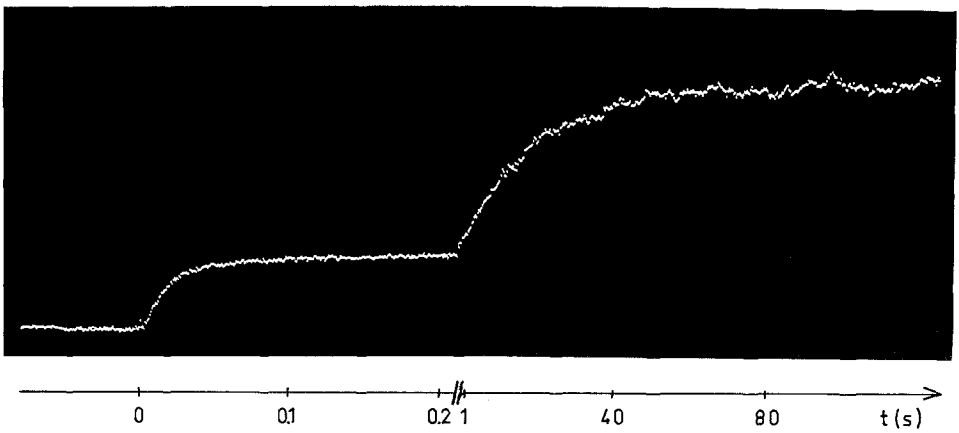

Fig. 6. Flash-induced near infrared scattering change from a suspension of randomly oriented rod outer segments. Total scattering is approximated by measuring the transmission change in the angular range $0° \leq \theta \leq 2°$; the flash was applied at $t = 0$. Under these conditions, the *ms*-signal *P* and the *s*-signal P_S are distinguished; a more detailed analysis of the fast *P*-signal reveals *s*-shaped kinetics. Both signals saturate at a rhodopsin turnover of about 10%–15%

Fig. 8. It will be termed singal P_D. The kinetics of the signal are essentially first order; the fast components, which are observed in ROS, cannot be detected. The difference scattering curve of the disc signal is shown in Fig. 7 together with the ROS-curves. The slight increase of the curve with increasing θ was, in other preparations, generally less pronounced. In all cases, the difference scattering for $\theta \rightarrow 0$ was the same.

In contrast to the monophasic signal of the disc vesicles, on ROS fragments, produced by an osmotic shock of 10 min in 10 mM KCl and reloaded with the protein extract, a *P*-signal with fast and slow kinetic components is obtained.

The essential result of these experiments with isotropic samples is, that the ROS structure is necessary for the light-scattering indication of the physical processes seen in the fast *P*-signal. As suggested by the difference scattering curve these processes are somehow connected with shifts of the scattering mass within the ROS.

In order to investigate more quantitatively the geometry and extent of these effects, experiments with axially oriented ROS were performed.

2. Axially Oriented Rod Outer Segments

Oriented ROS were measured with the device shown in Fig. 1b. The scattering intensity was recorded simultaneously in vertical and horizontal direction. For perfectly oriented ideal cylinders, pure radial and axial scattering would be observed in these directions.

The slow and fast signals behave quite differently under these conditions and are therefore considered separately.

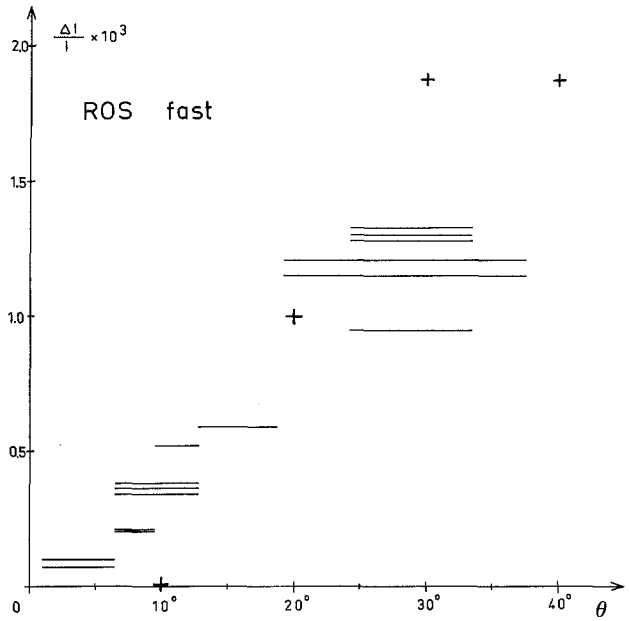
$\frac{\Delta I}{I} \times 10^3$
ROS fast
2.0
1.5
1.0
0.5
0
10°
20°
30°
40°
θ

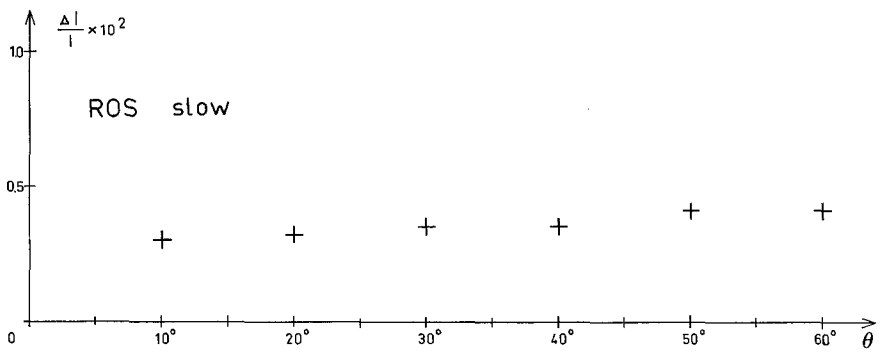
$\frac{\Delta I}{I} \times 10^2$
ROS slow
1.0
0.5
0
10°
20°
30°
40°
50°
60°
θ

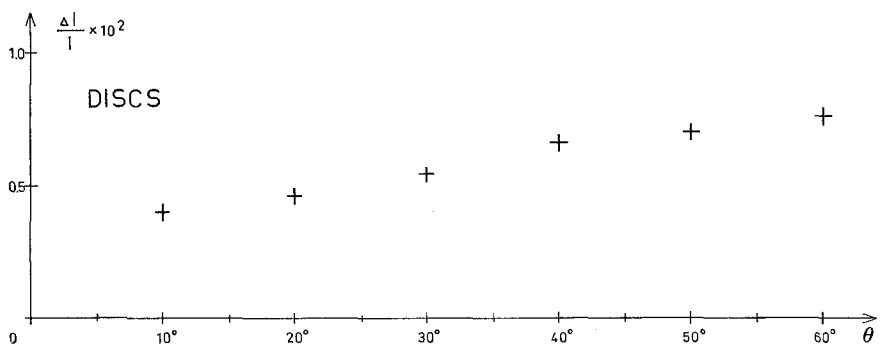
$\frac{\Delta I}{I} \times 10^2$
DISCS
1.0
0.5
0
10°
20°
30°
40°
50°
60°
θ

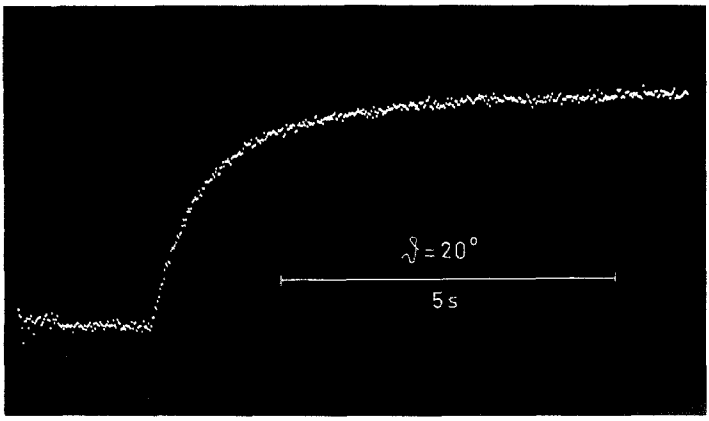

Fig. 8. Flash-induced near-infrared scattering change from a suspension of isolated disc vesicles, reloaded with the extracted proteins. Discs were prepared after Smith et al. (1975) and recombined with the extract of the peripheral proteins after Kühn (1981). Saturation and kinetics are dependent on the amount of protein added (see text). Note that the signal is nearly monophasic, by a factor of 25 slower than the fast P-signal and by a factor of 20 faster than the slow P_S-signal in ROS. Also in other experiments, we didn't find faster signal components under these conditions

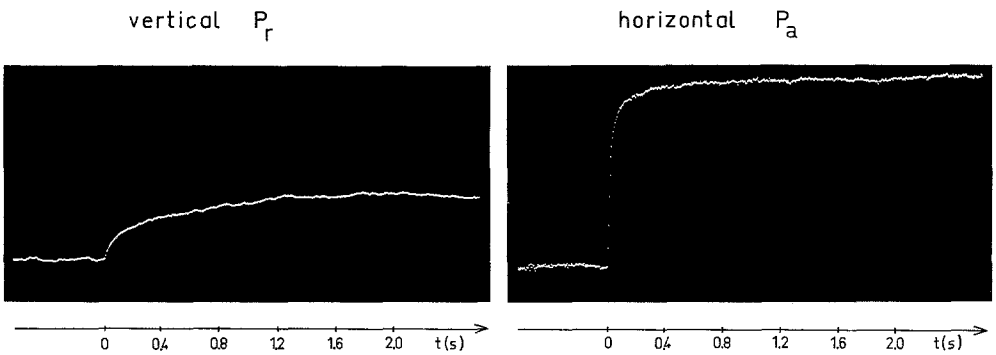

Fig. 9. Fast signal P of a suspension of axially oriented ROS; simultaneous measurement in vertical (P_r) and horizontal (P_a) direction. Horizontal orientation of the ROS axes; signals are the normalized intensity changes $\Delta I/I$; transmitted angular range $15° \leq \theta \leq 25°$. It is seen that the signal P (see Fig. 2) splits into two kinetically different signals

---

Fig. 7. Experimental difference scattering curves – angular dependence of the signal amplitudes for the signals P (above), P_S (medium), and P_D (below). For the signal P, a steep increase of the curve and an approximation to zero for $\theta \rightarrow 0$ is seen. The horizontal bars indicate the angular range transmitted in the optical arrangement in Fig. 1a; crosses are measurements with the optics in Fig. 1c. In contrast to the curve for the fast signal P seen in ROS, the slow ROS-signal P_S as well as the curve for the disc-signal P_D are flat; a constant function of θ was always found for P_S. The P_D-curve shown here is the most pronounced angular dependence which was found so far. Note the close quantitative relation between the disc effect P_S and the slow ROS-effect P_D

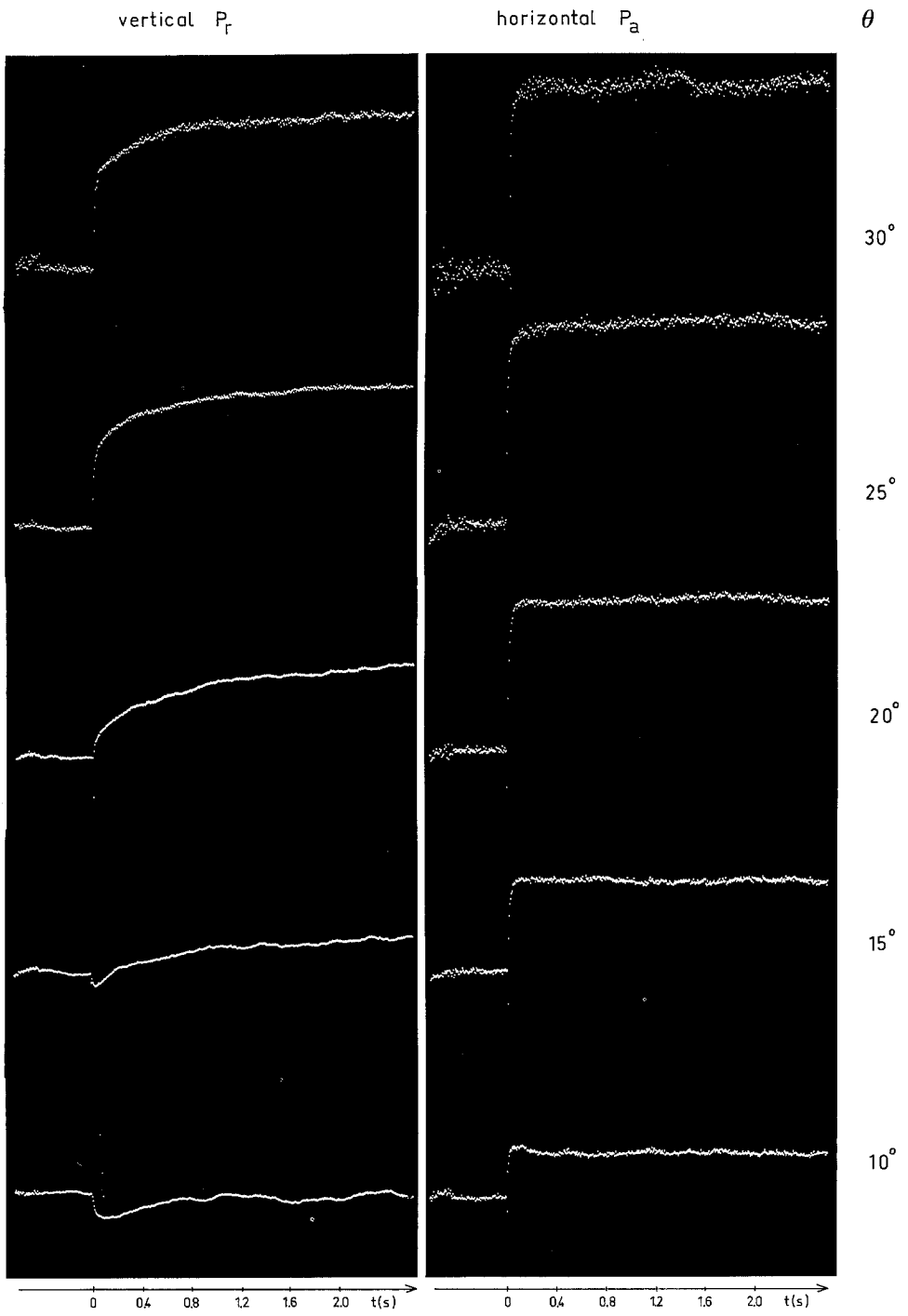
vertical P_r
horizontal P_a
θ
30°
25°
20°
15°
10°
0
0.4
0.8
1.2
1.6
2.0
t(s)

a) Slow Signal P_S. The slow signal is observed in the vertical and horizontal scattering, it is equal in size and kinetics to the signal P_S shown in Fig. 6. It is already known from the measurement of the isotropic sample that this signal has no dependence on θ. This was also verified with the oriented sample (not shown).

In measurements with linearily polarized monitoring light, the signal P_S was also independent of the orientation of the polarization vector relative to the orientation of the ROS axes.

b) Fast Signals P_r and P_a. Signals of oriented ROS in the ms range were measured simultaneously in the vertical and horizontal direction. In this measurement, a broad range of the scattering angles is transmitted in order to enhance the detected total intensity. As is seen in Fig. 9, two different effects are observed in the vertical and horizontal scattering. Under these conditions, the isotropic *P*-signal (Fig. 6) splits into two orientation-dependent components.

In spite of the deviations of the ROS from the cylindrical shape, the vertical scattering is preferently radial, the horizontal axial. Therefore, the terms P_r and P_a will be used for the slow vertical and the fast horizontal signal.

The splitting depends on the quality of the preparation, being higher, the higher the anisotropic ratio of the sample; for preparations with a ratio of 4 (for example frozen and thawed preparation, Table 1), two more similar signals with kinetics intermediate between P_r and P_a are observed.

In Fig. 10, a measurement with sharper angular selection is shown. For every angle, the horizontal and vertical scattering changes are measured simultaneously. Due to the sharp selection of the scattered light, large fluctuations are superimposed to the signals.

The overall picture is essentially similar to Fig. 9 at all scattering angles: in the vertical scattering, a distinct slow signal is seen, in horizontal direction a fast signal; both effects increase with increasing θ, as did the signals of the isotropic sample (Fig. 7). A more detailed consideration also shows that at small angles a fast negative vertical effect is superimposed to the slow vertical signal. With increasing angle, a fast positive component becomes predominant. In the wider angular range of the measurement in Fig. 9, these fast effects were just compensated and only the positive signals P_r and P_a were observed.

In order to perform a quantitative evaluation, the orientation and angular-dependent measurement was repeated with a number of fresh preparations. Up to four measurements with fresh samples from one preparation were averaged. For several samples, the measured difference scattering of P_r and P_a is shown in Fig. 11. It is seen that the absolute values of the signal

---

Fig. 10. Fast signal *P* of a suspension of axially oriented ROS. Simultaneous measurement in vertical and horizontal direction. Different samples from the same preparation for the measurements at the different angles. Horizontal orientation of the ROS-axes, the vertical effect is therefore essentially radial (P_r), the horizontal effect axial (P_a). Signals are the normalized intensity changes $\Delta I/I$. Transmitted angular range $\theta \pm 2°$. Apart from superimposed negative and positive side effects in the vertical scattering, the signals P_r and P_a, both increasing with θ, are seen

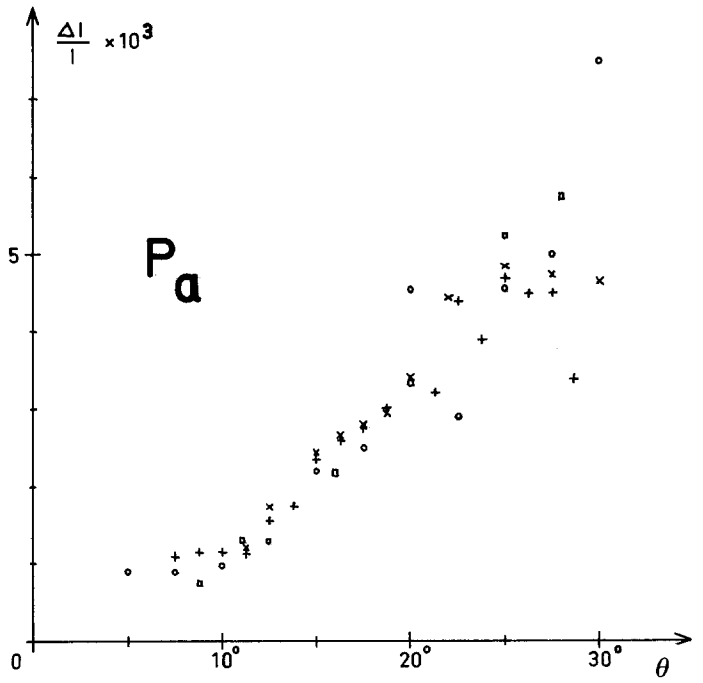
Δl/l ×10³
Pa
5
0
10°
20°
30°
θ

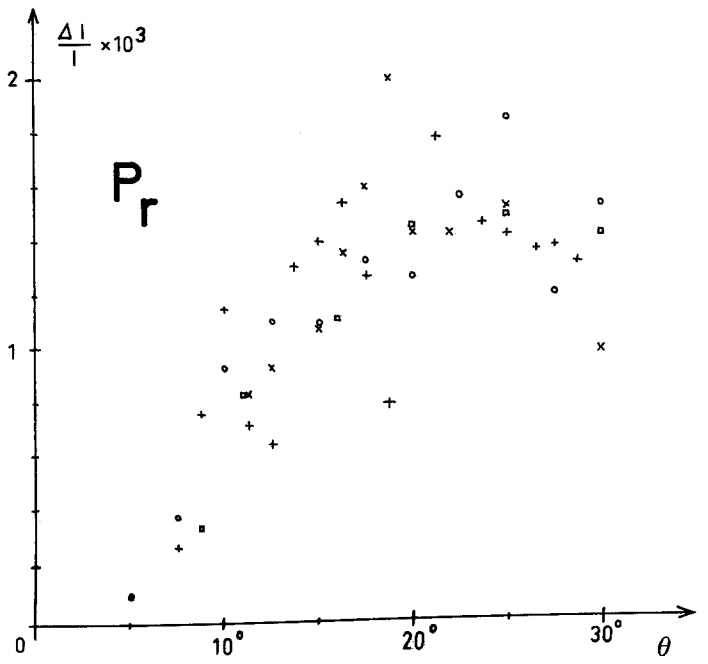
Δl/l ×10³
Pr
2
1
0
10°
20°
30°
θ

amplitudes coming from different preparations fit together. The overall curve of P_a points to zero for $\theta \to 0$.

In the case of P_r, it appears noteworthy to mention how the P_r-amplitudes were evaluated. One of the large signals obtained at higher scattering angles was taken as a standard. The other signals were fitted to this signal in a certain region of addresses with the continuous digital scale expansion of the signal analyzer. The expansion factor yields the amplitude. In spite of this procedure, not all measurements at small angles could be evaluated because of the large amplitude of sample fluctuations in this range. There are, therefore, only few measuring points for $\theta < 10°$. However, an overall decrease of the amplitude with decreasing θ can be stated. For the behaviour of P_r at small θ, additional evidence comes from the finding that the isotropic curve (Fig. 7) approximates to zero or small negative values for $\theta \to 0$. Any larger deviation of P_r from this behaviour would have to be compensated by non-zero contributions of P_a, but this is not measured. An upper limit for the relative intensity change of P_r for $\theta \to 0$ is $\Delta I/I = -2 \times 10^{-3}$ (Figs. 7 and 11). This value is by a factor of ten smaller than those for P_S and P_D (Fig. 7).

Discussion

1. Scattering Interpretation

The measurements with randomly oriented ROS (Figs. 6 and 7) show that the theoretical cases [formulae (6) and (8)] are actually found in the real sample: The difference scattering curve of the *P*-signal (Fig. 7) suggests a non-local shift of the scattering mass, whereas that of the P_S-signal (Fig. 7) corresponds to a local (extension < 500 Å, see theory) change of the refractive index directly seen in light-scattering.

It is noteworthy that the non-local mass shift effects have apparently no refractive index change as a local counterpart: the non-local shifts, therefore, are caused by local processes which cannot be detected directly. This means a selection with respect to their molecular interpretation.

A relation of the slow P_S-signal observed in ROS to the signal P_D found in discs is suggested by their common physical interpretation as local scattering effects. The quantitative correspondence between the relative intensity changes is, however, only accidental since P_D depends on the amount of recombined protein. The relative intensity changes being ca. 10^{-2} (Fig. 7), a relative change of the refractive index of ca. 10^{-4} is calculated using formula (6). Comparing the

---

Fig. 11. Experimental difference scattering curves – angular dependence of the signal amplitudes for the signals P_r and P_a (compare Fig. 10). In both cases, the absolute values of the actually measured signal amplitudes are plotted; the different symbols are different preparations. The upper curve is obviously not constant and appears to point to zero for $\theta \to 0$; for the lower curve, the angular dependence is not so clear since only few reliable measuring points for $\theta < 10°$ are available. Compare P_r to the radial and P_a to the axial difference scattering of ideal particles shown in Fig. 3. See text for the details

relative intensity changes to those observed in temperature-induced phase transitions of phosphatidic acid (Eibl and Blume 1979) or lecithin (Chong and Colbow 1976) vesicles, the light-induced effects are estimated as about 5% of the temperature-induced effects.

In the measurements with axially oriented ROS, the fast signal is splitted into an axial and a radial component with different kinetics. A comparison of the experimental curves with the calculated transfer functions in Fig. 2 allows the following estimations:

1. The radial as well as the axial signal are positive intensity changes and, therefore, both represent a decrease of the scattering center distances within the particle (negative values of γ in the whole angular range).
2. The curve of the radial signal P_r is comparable to the theoretical curve of a change of the radius; taking into account the morphology of the ROS, it appears that the scattering centers move closer together within the plane of the disc membranes, with the result of a change of the mean scattering radius. We cannot decide from these data whether only parts of the membranes are involved or if the whole membranes shrink. If the latter is assumed, a relative shrinkage of $\Delta R/R = \Delta I/I \cdot \gamma \approx 1.2 \times 10^{-3}$ is obtained for the 2.0% bleaching in this experiment.
3. Concerning the axial effect P_a, the comparison with the theoretical curve in Fig. 2 shows that the accordance would be satisfying for a curve which represents an axial dimension of 1–2 μm. This is in contrast to the absolute scattering curve which indicates the transformation of a 5–10 μm dimension into scattering without major deviations from the Rayleigh-Gans-approximation. It appears that it is the sample itself which is coherent (with respect to the axial shrinkage) only in an average dimension of ca. 2 μm. The problem is only important for the quantitative estimation of the axial shrinkage: if packets of discs sticking together with an average length of 2 μm are assumed, a relative axial shrinkage of $\Delta L/L = \gamma \cdot \Delta I/I \approx 1.5 \times 10^{-2}$ is obtained.

As a consequence of the imperfect cylindrical shape of the ROS, a certain 'crosstalk' between vertical and horizontal effects has to be expected. It appears that such an effect is actually observed in the smaller but quite pronounced fast effect in vertical direction, which increases parallel to the fast signal P_a.

The negative effect which becomes distinct at small angles in the vertical direction, is by a factor of 3 larger than the theoretically (and experimentally, signal at $\theta = 0$) expected total scattering signal. So far, we have no interpretation for the remaining negative signal.

Apart from these side effects, the signals found in this study can be summarized as shown in Table 2.

2. *Possible Molecular Origin of the Signals*

Whereas in the ROS three different signals are found, one single signal is observed in discs. This could simply be caused by the lack of indicators for the axial and radial shrinkage. This explanation is obvious for the axial effect since the thickness of the single discs is too small to be indicated in light-scattering. It

Table 2. Summary of the signals

	Symbols	Time const.	Ref. in Fig.	Interpretation	Extent for 1% bleaching
Rod outer segments	P_a	10 ms	9	Axial shrinkage	$\Delta L/L \approx 1 \times 10^{-2}$
	P_r	50–100 ms	9	Radial shrinkage	$\Delta R/R \approx 5 \times 10^{-4}$
	P_S	5–25 s	6	Change of refractive index	$\Delta n/n \approx 1 \times 10^{-4}$
Discs	P_D	0.6–1.2 s	8	Change of refractive index	$\Delta n/n \approx 1 \times 10^{-4}$

is, however, also conceivable for the radial effect because of the irregular curvature of the disc planes after isolation.

We cannot decide from the scattering data whether the underlying molecular events or if merely the indicators are affected by the isolation of the discs.

For the present discussion, it is sufficient to know, that in the one of the investigated systems (which is closer to the natural state) three kinetically and physically different effects are found.

Very recently, Kühn et al. (1981) found a close relation between the binding of GTPase to rhodopsin and a near-infrared transmission change with complicated multiphasic kinetics and the illumination dependence of the effects discussed here. The authors describe a proportionality between the saturation level of their signal and the amount of GTPase added to their disc membrane preparation.

Preliminary experiments in our laboratory suggest a more complex relation between the different *P*-signal types and the GTPase: Adding protein extract to the disc preparation, we also observed the proportionality found by Kühn et al. in the case of the signal P_D. Overloading, however, fresh ROS with the proteins extracted (Kühn 1978) from another aliquot of the same preparation, we could not find any influence on the shrinkage signals P_r and P_a. Under these conditions, a new signal is observed, which is comparable to P_D in its kinetics and saturation.

On the other hand, an indication that the GTPase is involved in P_r was found in the strong decrease of the latter with decreasing ionic strength (for P_a much less pronounced). The dependence is approximately parallel to the binding of GTPase on fresh ROS (Kühn 1981). It appears conceivable that P_r reflects a special mode of reaction between rhodopsin and GTPase which exists only for GTPase concentrations within the natural range and is replaced by the P_D-like mode for higher concentrations.

One might therefore tentatively assume, that the radial shrinkage seen in P_r is summed up by local contributions of single GTPase-complexes within the fluid coherent disc membrane planes. With $\Delta R/R \approx 5 \times 10^{-4}$ for a bleaching of 1% (Table 2), the area decrease is calculated as:

$$dA = 2\,R^2\pi \cdot 5 \cdot 10^{-4} \approx 10^5\ \text{Å}^2\,.$$

1% of the rhodopsin within one disc membrane being ca. $2.5 \cdot 10^2$ molecules, the area decrease per bleached rhodopsin would be estimated as 450 Å^2. This value for the ideal cylinder is an upper limit. A real estimation for the curved ROS is 300 ± 100 Å^2.

This value is very high and it is tempting to speculate that the GTPase is lifted or turned during the signal P_r.

In this kind of process, only weak local interactions would be involved, as it must be assumed in view of the fact that the mass shift seen in P_r has no local concomitant.

Appendix

The "*particle scattering function*" or "form factor" in (3) shall now be considered. Note that this is the case of an unpolarized incident beam. The function for cylinders can be written as a product of a radius- and a length-dependent term (van de Hulst 1957):

$$P(\theta) = 4 \cdot \underbrace{\frac{J_1^2(sR\sin\beta)}{(sR\sin\beta)^2}}_{F^2(u)} \cdot \underbrace{\frac{\sin^2\left(\frac{sL}{2}\cos\beta\right)}{\left(\frac{sL}{2}\cos\beta\right)^2}}_{E^2(u)} \tag{A1}$$

with $s = \frac{4\pi}{\lambda}\sin\theta/2$.

R radius; L length; J_1 first order Bessel function.

β is the angle between the cylinder axis and the bisectrix between incident and scattering direction. The two terms in (A1) arise from integrations with respect to the radial resp. axial dimension of the particle.

A geometrical consideration, which is also given by van de Hulst, transforms β into the experimentally more convenient parameters α (angle between incident beam and cylinder axis), ϕ (rotation of the axis around the optical axis) and θ (scattering angle). One obtains:

$$\cos\beta = -\cos\alpha \cdot \sin\theta/2 + \sin\alpha \cdot \cos\theta/2 \cdot \cos\phi \, . \tag{A2}$$

The equations for the axially oriented and randomly oriented sample can now be deduced from (A1) and (A2).

Concerning the axially oriented sample, we are only interested in the case of perpendicular incidence ($\alpha = 90°$) and of horizontally oriented axes (compare Fig. 1b). The vertical scattering ($\phi = 90°$, $\alpha = 90° \rightarrow \cos\beta = 0$) function is then

$$P_v(\theta) = 4 \cdot \frac{J_1^2(sR)}{(sR)^2} \, . \tag{A3}$$

For the horizontal scattering ($\phi = 0°$, $\alpha = 90° \rightarrow \cos\beta = \cos\theta/2$ one obtains:

$$P_h(\theta) = 4 \cdot \frac{J_1^2(sR \cdot \sin\theta/2)}{(sR \cdot \sin\theta/2)^2} \cdot \frac{\sin^2\left(\frac{sL}{2} \cdot \cos\theta/2\right)}{\left(\frac{sL}{2} \cdot \cos\theta/2\right)^2}. \tag{A4}$$

It is seen from (A3) and (A4) that the length of the cylinder does not influence the solution $P_v(\theta)$ for the vertical scattering; this finding can be used to estimate the influence of the cylinder length on the scattering anisotropy P_v/P_h. The horizontal scattering $P_h(\theta)$ is only very slightly modulated by the radius-dependent first term. Therefore, the horizontal scattering can be regarded as axial, the vertical scattering as radial.

For the scattering of the randomly oriented cylinders, one has to integrate over all directions

$$P(\theta) = 4 \cdot \int_0^1 \frac{J_1^2(sR\sqrt{1-y^2})}{(sR\sqrt{1-y^2})^2} \cdot \frac{\sin^2\left(\frac{sL}{2}y\right)}{\left(\frac{sL}{2}y\right)^2} dy \tag{A5}$$

with $y = \cos\theta/2$.

The *transfer functions* defined in (5) will be obtained following the general Eq. (7). One obtains for the oriented cylinders the following solutions:
horizontal scattering, change of the length (index *Lh*):

$$\gamma_{Lh} = 2\left(\frac{sL\cos\theta/2}{\tan(sL\cos\theta/2)} - 1\right) \tag{A6}$$

vertical scattering, change of the radius:

$$\gamma_{Rv} = 2\left(sR\frac{J_0(sR)}{J_1(sR)} - 2\right) \tag{A7}$$

γ_{Rh} can be neglected in the considered angular range and γ_{Lv} is exactly zero, as is also seen from the geometry of the scattering given in (A3) and (A4). The functions γ_{Lh} and γ_{Rv} are shown in Fig. 2.

For the case of random orientation, one has to differentiate under the integral in (A5) and obtains for a change of the length:

$$\bar{\gamma}_L(\theta) = \frac{L}{P(\theta)} \cdot 4 \cdot \int_0^1 \frac{J_1^2(sR\sqrt{1-y^2})^2}{(sR\sqrt{1-y^2})^2} \cdot 8 \cdot \frac{\left(\cos\frac{sLy}{2}\sin\frac{sLy}{2}\right)\frac{sLy}{2} - \sin^2\frac{sLy}{2}}{s^2L^3y^2} dy \tag{A8}$$

and for a change of the radius

$$\bar{\gamma}_R(\theta) = \frac{R}{P(\theta)}$$
$$\cdot 4 \int_0^1 \frac{-4 J_1^2(sR\sqrt{1-y^2}) + 2\, sR\sqrt{1-y^2} \cdot J_1(sR\sqrt{1-y^2}) \cdot J_0(sR\sqrt{1-y^2})}{s^2R^3\sqrt{1-y^2}}$$
$$\cdot \frac{\sin^2\left(\frac{sLy}{2}\right)}{\left(\frac{sLy}{2}\right)^2} dy\,. \tag{A9}$$

For the estimation of the *lamellarity* influence, one starts with the L-dependent term in (A1). This term has the form $\sin u/u$ and arises from an integration with respect to the length. The modulation of the refractive index has to be introduced into this integration:

$$E'(u, {}^1/_d) = \frac{1}{L} \int_{-L/2}^{+L/2} e^{2ik \sin\theta/2 \cos\beta \cdot z} \cdot \left[1 + b \cos\left(2\pi \frac{z}{d}\right)\right] dz\,. \tag{A10}$$

The real part of E' is calculated:

$$E'(u, v) = \frac{\sin u}{u} + \frac{b}{2} \frac{\sin(u+v)}{(u+v)} + \frac{b}{2} \frac{\sin(u-v)}{(u-v)} \tag{A11}$$

with $u = (sL/2) \cos\beta$, $v = \pi L/d$.

It is seen that this solution does not deviate from the homogeneous case if $u \ll v$, i.e., $d \ll \lambda$.

Acknowledgements. We wish to thank Prof. W. Kreutz, Prof. H. Rüppel and Dr. F. Siebert for valuable discussions, as well as Mrs. W. Herbst and Miss C. Aehnelt for critical reading the manuscript and Miss S. Filter for the typescript.

Financial support from the Deutsche Forschungsgemeinschaft (SFB 70, A 7) is gratefully acknowledged.

References

Bauer PJ, Mavromati E (1980) Interaction of Ficoll with bovine disc membranes. Biophys Struct Mech [Suppl] 6: 116

Chabre M (1975) X-ray diffraction studies of retinal rods. I. Structure of the disc membrane, effect of illumination. Biochim Biophys Acta 382: 322–335

Chabre M (1978) Diamagnetic anisotropy and orientation of alpha-helix in frog rhodopsin and meta II-intermediate. Proc Natl Acad Sci USA 75: 5471–5474

Chong CS, Colbow K (1976) Light-scattering and turbidity measurements on lipid vesicles. Biochim Biophys Acta 436: 260–282

Eibl H, Blume A (1979) The influence of charge on phosphatidic acid bilayer membranes. Biochim Biophys Acta 553: 476–488

Farone WA, Kerker M, Matijević E (1963) Scattering by infinite cylinders at perpendicular incidence. In: Kerker M (ed) Interdisciplin Conf Electromagn Scatt. Pergamon Press, New York

Hofmann KP, Uhl R, Hoffmann W, Kreutz W (1976) Measurements of fast light-induced light-scattering and -absorption changes in rod outer segments of vertebrate light sensitive rod cells. Biophys Struct Mech 2: 61–77

Hofmann KP, Emeis D (1981) Comparative kinetic light-scattering and -absorption photometry. Biophys Struct Mech 8: 23–34

Hulst HC van de (1957) Light-scattering by small particles. J Wiley and Sons, New York; Chapman and Hall, London

Kerker M (1969) The scattering of light and other electromagnetic radiation. Academic Press, New York London

Kratochvil P (1972) Particle scattering functions. In: Huglin MB (ed) Light-scattering from polymer solutions. Academic Press, New York

Kühn H (1978) Light-regulated binding of rhodopsin kinase and other proteins to cattle photoreceptor membranes. Biochemistry 17: 4389–4395

Kühn H (1981) Personal communication

Kühn H, Bennett N, Michel-Villaz M, Chabre M (1981) Interactions between photoexcited rhodopsin and GTP binding protein: kinetic and stoichiometric analysis from light-scattering changes. Proc Natl Acad Sci USA (in press)

Liebman PA, Jagger WS, Kaplan MW, Bargoot FG (1974) Membrane structure changes in rod outer segments associated with rhodopsin bleaching. Nature 251: 31–36

Mie G (1905) Beiträge zur Optik trüber Medien, speziell kolloidaler Metall-Lösungen. Ann Phys 25: 379–445

Norisuye T, Yu H (1977) Osmotically induced and photo-induced deformations of disc membranes. Biochim Biophys Acta 47: 436–452

Smith HG Jr, Stubbs GW, Litman BJ (1975) The isolation and purification of osmotically intact discs from retinal rod outer segments. Exp Eye Res 20: 211–217

Uhl R, Hofmann KP, Kreutz W (1977) Measurement of fast light-induced disc-shrinkage within bovine rod outer segments by means of a light-scattering transient. Biochim Biophys Acta 469: 113–122

Received November 13, 1980/Accepted September 21, 1981